

Electron tunneling spectroscopy of an anisotropic Kitaev quantum spin liquid sandwiched between superconductors

Shi-Qing Jia  and Liang-Jian Zou *

Key Laboratory of Materials Physics, Institute of Solid State Physics, HFIPS, Chinese Academy of Sciences, Hefei 230031, China
and Science Island Branch of Graduate School, University of Science and Technology of China, Hefei 230026, China

Ya-Min Quan 

Key Laboratory of Materials Physics, Institute of Solid State Physics, HFIPS, Chinese Academy of Sciences, Hefei 230031, China

Xiang-Long Yu

Shenzhen Institute for Quantum Science and Engineering, Southern University of Science and Technology, Shenzhen 518055, China
and International Quantum Academy, Shenzhen 518048, China

Hai-Qing Lin[†]

Beijing Computational Science Research Center, Beijing 100193, China
and Department of Physics, Beijing Normal University, Beijing 100875, China



(Received 10 March 2021; revised 27 March 2022; accepted 3 June 2022; published 28 June 2022)

We present the electron tunneling transport and spectroscopic characters of a superconducting (SC) Josephson junction with a barrier of a single anisotropic Kitaev quantum spin liquid (QSL) layer. We find that the dynamical spin-correlation features are well reflected in the direct-current differential conductance dI^c/dV of single-particle tunneling, including the unique spin gap and dressed itinerant Majorana dispersive band, in addition to an energy shift 2Δ from the two-SC-lead gap. From the spectral characters, we identify different topological quantum phases of the anisotropic Kitaev QSL. We also present the zero-voltage Josephson current I^s , which displays residual features of the anisotropic Kitaev QSL. These results pave a new path to measurement of dynamical spinon or Majorana fermion spectroscopy of Kitaev and other spin-liquid materials.

DOI: [10.1103/PhysRevResearch.4.023251](https://doi.org/10.1103/PhysRevResearch.4.023251)

I. INTRODUCTION

Quantum spin liquids (QSLs), which consist of various spin quantum states without breaking any constituent symmetries of the underlying lattice, have attracted great attention [1,2]. Enormous effort has been expended in attempting to understand the essence of QSLs, and earlier studies have focused on geometrically and magnetically frustrated interactions [3,4]. However, the essence and unique characters of QSL states remain the subject of great debate [5,6]. More than a decade ago, Kitaev proposed an exactly solvable model on a two-dimensional (2D) honeycomb lattice [7], and this shows that the interaction frustration drives a ground state of a gapless or gapped Z_2 QSL with fractionalized excitations [8]. The QSL state with gapped excitations has Abelian anyons [9], and the state with gapless excitations may have non-Abelian

anyon excitations [10]. Due to topological protection and the large degeneracy of these anyons, the Majorana fermion excitations and the braiding group in the gapless QSL state are expected to be applicable to quantum computing storage and quantum computation [8,11]. However, researchers have not yet found ways in which to excite and detect the dynamics of these Majorana fermion modes in Kitaev systems.

Josephson tunneling junctions, which consist of two superconducting (SC) leads separated by an insulating or metallic barrier, provide a good probe for measuring quasiparticle information from the central region through quantum tunneling transport [12,13]. A large number of central materials have been studied, including insulators [14], normal metals [15], quantum dots [16–18], ferromagnets [19–21], and antiferromagnets [22,23]. To explore the exotic spin correlations and fractional excitations of Majorana fermions through the transport of single electrons and Cooper pairs, especially the inelastic spin-scattering process [24–26], it is worth constructing novel SC–Kitaev layer–SC tunneling junctions to reveal the current dynamics associated with exotic spin excitations in the Kitaev layer. In the realistic candidate materials for the Kitaev layer, spin interactions are usually anisotropic [27–30]; therefore here we employ anisotropic Kitaev layers in the designed SC Josephson junctions.

*zou@theory.issp.ac.cn

†haiqing0@csrc.ac.cn

Published by the American Physical Society under the terms of the [Creative Commons Attribution 4.0 International](https://creativecommons.org/licenses/by/4.0/) license. Further distribution of this work must maintain attribution to the author(s) and the published article's title, journal citation, and DOI.

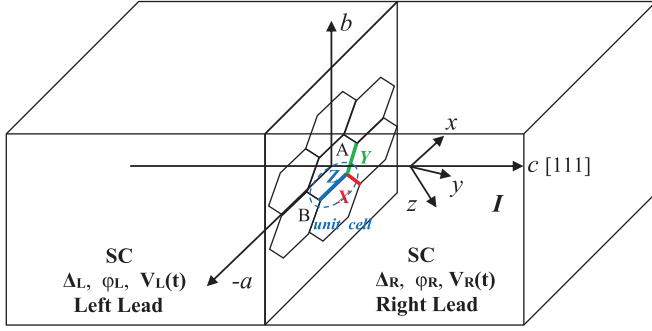


FIG. 1. Schematic diagram of a SC–Kitaev QSL–SC tunneling junction. The left (right) side is an SC lead with gap Δ_L (Δ_R), phase ϕ_L (ϕ_R), and electric potential $V_L(t)$ [$V_R(t)$]. The central region is a single-layer Kitaev material in the ab plane.

In this paper, we use the current and conductance features of SC–anisotropic Kitaev layer–SC tunneling junctions to characterize the dynamical spin correlations of the central-zone Kitaev materials. We adopt the nonequilibrium Green’s function [17] and the few-particle response method [31,32] to obtain formulas for the single-particle and Josephson tunneling currents. We find that the dynamical spin susceptibility is explicitly displayed in the direct current (DC) single-particle differential conductance spectrum dI^c/dV , and from its spectral features, we can confirm the different topological quantum phases of the anisotropic Kitaev QSL. It is expected that SC–anisotropic Kitaev QSL–SC mesoscopic hybrid systems with weak links may be a fruitful research field not only because of the abundant fundamental features obtained from the interplay between Kitaev physics and SC but also because of their potential applications in the design and development of new quantum devices.

II. MODEL AND TUNNELING OF THE SC–KITAEV QSL–SC JUNCTION

A. The SC–Kitaev QSL–SC junction and tunneling process

We construct a Kitaev Josephson junction in which a single-layer Kitaev insulator is the barrier, and this is sandwiched by two leads consisting of conventional s -wave SCs. Here the SC leads may be made from Nb or Pb or their alloys, such as NbTi or Nb₃Sn, and the central Kitaev layer may be a single layer of α –RuCl₃ or Na₂IrO₃, which are Kitaev QSL candidate materials [29]. A schematic of such an SC–Kitaev QSL–SC Josephson junction is shown in Fig. 1. Since the Kitaev material is a kind of transition-metal Mott insulator with a strong electronic correlation, the tunneling of conduction electrons between the left and the right SC leads is scattered by the local spins in the central region, as shown in Fig. 2. The scattering strength is that of the s – d -type exchange coupling J .

For this setup, the tunneling current consists of the normal single-particle and Josephson contributions. We can describe the normal single-particle tunneling process as follows. First, the electrons at the bottom of the SC gap in the right lead enter the Kitaev layer, and they occupy the high-energy levels to form virtual double-occupied states. The propagation of the electrons would be modulated by the dynamical spin

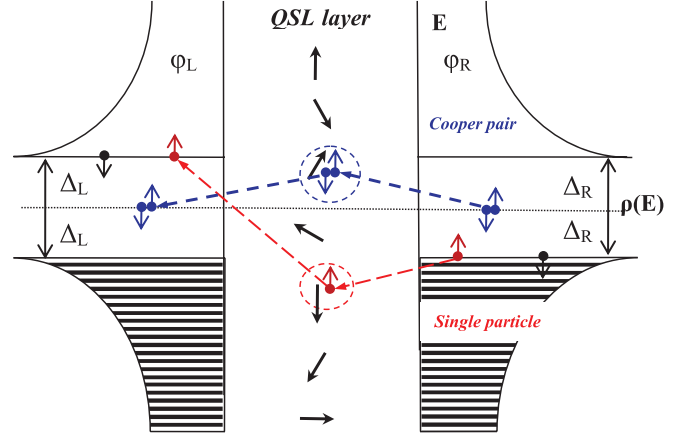


FIG. 2. Sketch diagram of single-particle (red) and Cooper-pair (blue) tunneling processes in a SC–Kitaev QSL–SC Josephson junction. The left and right sides show the bare DOS distributions $\rho(E)$ of the two SC leads, and the central region is the Kitaev QSL layer. The circles indicate the s – d exchange processes of a single particle and a Cooper pair with local spin.

susceptibility of the Kitaev QSL in the spin-conserving channel as well as in the spin-flipping process with spin fluctuations. Finally, the electrons leave the Kitaev layer with constant or opposite spins and proceed to the top of the SC gap in the left SC lead.

The tunneling process of the SC Cooper pairs can be addressed as follows. A Cooper pair in the right lead first tunnels into the central Kitaev region, splitting into a quasielectron and quasihole with opposite spins. After this, the quasielectron and quasihole would go through similar virtual transitions as single particles with the modulation of the Kitaev QSL. Once they have tunneled out of the central Kitaev region, the separated quasielectrons and quasiholes would recombine into SC Cooper pairs. These tunneling processes can be qualitatively described by the sketch diagram shown in Fig. 2.

B. Model Hamiltonian and formulas

The total Hamiltonian of the SC–Kitaev QSL–SC tunneling junction shown in Figs. 1 and 2 consists of three parts: The left and right SC electrodes $H_{\text{Lead},n}$ ($n = L, R$), the single-layer Kitaev material in the central scattering region H_{cen} , and the s – d exchange interaction part between the SC leads and the central material H_T . Thus $H = \sum_{n=L,R} H_{\text{Lead},n} + H_{\text{cen}} + H_T$, and

$$H_{\text{Lead},n} = \sum_{k\sigma} \epsilon_{nk\sigma}^0 a_{nk\sigma}^\dagger a_{nk\sigma} + \sum_k \Delta_n [a_{n,-k\downarrow} a_{nk\uparrow} + \text{H.c.}],$$

$$H_{\text{cen}} = -K_X \sum_{\langle ij \rangle_X} \hat{\sigma}_i^x \hat{\sigma}_j^x - K_Y \sum_{\langle ij \rangle_Y} \hat{\sigma}_i^y \hat{\sigma}_j^y - K_Z \sum_{\langle ij \rangle_Z} \hat{\sigma}_i^z \hat{\sigma}_j^z, \quad (1)$$

$$H_T = \sum_i \left\{ \frac{-\tilde{J}_i(t)}{2} \left[\hat{\sigma}_i^z (a_{Li\uparrow}^\dagger a_{Ri\uparrow} - a_{Li\downarrow}^\dagger a_{Ri\downarrow}) + \hat{\sigma}_i^+ a_{Li\uparrow}^\dagger a_{Ri\uparrow} + \hat{\sigma}_i^- a_{Li\downarrow}^\dagger a_{Ri\downarrow} \right] + \text{H.c.} \right\},$$

where $a_{nk\sigma}^\dagger$ and $c_{i\sigma}^\dagger$ are the creation operators of electrons in the SC leads and Kitaev layer, respectively, and $a_{ni\sigma}^\dagger$ is the Fourier transform of $a_{nk\sigma}^\dagger$ on the i th site of the 2D

interface between the SC leads and the Kitaev layer; $\hat{\sigma}_i^{x(y,z)} = \sum_{\sigma\sigma'} c_{i\sigma}^\dagger \sigma_{\sigma\sigma'}^{x(y,z)} c_{i\sigma'}$ are twice the spin components; and $\hat{\sigma}_i^\pm = \hat{\sigma}_i^x \pm i\hat{\sigma}_i^y$, where $\sigma_{\sigma\sigma'}^{x(y,z)}$ are the Pauli matrices. Let the two SC leads be the s -wave SCs, their order parameters are $\tilde{\Delta}_n = \Delta_n e^{-i\phi_n}$ with magnitudes Δ_n and phases ϕ_n , and $\epsilon_{nk\sigma}^0$ is the single-electron energy. K_X , K_Y , and K_Z are the spin-coupling constants along the X , Y , and Z bonds in the central Kitaev layer, and these satisfy the conditions $K_X = K_Y > 0$ and $K_X + K_Y + K_Z = 3K$ for the anisotropic Kitaev model. J_i is the s - d exchange matrix element between the electrons in the SC leads and the local spins in the Kitaev layer. In the presence of an external electric potential $V_n(t)$ ($n = L, R$), the exchange parameter becomes the voltage dependence of $\tilde{J}_i(t) = J_i \exp[i(\phi_L - \phi_R) - (i/\hbar) \int_0^t e(V_L(t_1) - V_R(t_1)) dt_1]$ through a unitary transformation, leaving only the perturbation term H_T that explicitly depends on time [16].

The tunneling current from the left SC lead to the central region reads

$$I(t) = -e \left\langle \frac{dN_L(t)}{dt} \right\rangle = \frac{ie}{\hbar} \langle [N_L(t), H(t)] \rangle \\ = -\frac{e}{\hbar} \text{Re} \sum_i \tilde{J}_i(t) i \left\langle \begin{array}{l} \hat{\sigma}_i^z (a_{Li\uparrow}^\dagger a_{Ri\uparrow} - a_{Li\downarrow}^\dagger a_{Ri\downarrow}) \\ + \hat{\sigma}_i^+ a_{Li\downarrow}^\dagger a_{Ri\uparrow} + \hat{\sigma}_i^- a_{Li\uparrow}^\dagger a_{Ri\downarrow} \end{array} \right\rangle. \quad (2)$$

This actually contains two parts: The normal single-particle tunneling current and the SC Josephson current. Both of these stem from inelastic scattering with spin-conserving ($m = zz$) and spin-flipping ($m = xx, yy$) processes,

$$I(t) = -\frac{2e}{\hbar} \text{Re} \sum_{ij,m} \int_{-\infty}^t \frac{dt_1}{\hbar} J_i J_j \left\{ \begin{array}{l} e^{\frac{ieV(t-t_1)}{\hbar}} \left[\tilde{g}_{m,LR,ij}^r(t, t_1) G_{m,ji}^<(t_1, t) \right. \\ \left. + \tilde{g}_{m,LR,ij}^<(t, t_1) G_{m,ji}^a(t_1, t) \right] \\ + e^{\frac{ieV(t+t_1)}{\hbar}} e^{i\phi} \left[\tilde{g}_{m,LR,ij}^r(t, t_1) G_{m,ji}^<(t_1, t) \right. \\ \left. + \tilde{g}_{m,LR,ij}^<(t, t_1) G_{m,ji}^a(t_1, t) \right] \end{array} \right\}. \quad (3)$$

Throughout this paper, we only consider the DC voltage $V = V_L - V_R$, and $\phi = \phi_L - \phi_R$ is the phase difference between the left and the right SC leads. We define $G(g)^{r,a,<}(t_1, t)$ with the superscripts r , a and $<$ as the dressed (bare) retarded, advanced, and lesser Green's functions of spin correlation in the central region, respectively; $\tilde{g}_{m,LR,ij}^{r,a,<}(t, t_1)$ and $\tilde{g}_{m,LR,ij}^{r,a,<}(t, t_1)$ are bare normal and anomalous Green's functions of electron-hole modes and Cooper pairs between the left and right SC leads, respectively. For example, the advanced Green's functions can be written as:

$$g_{m,ji}^r(t_1, t) = -i\theta(t_1 - t) \langle [0.5\hat{\sigma}_i^x(t_1), 0.5\hat{\sigma}_i^y(t)] \rangle, \quad (4)$$

$$\tilde{g}_{m,LR,ij}^r(t, t_1) = -i\theta(t - t_1) \\ \langle [\hat{\sigma}_{\sigma\sigma'}^\alpha a_{Li\sigma}^\dagger a_{Ri\sigma'}(t), \hat{\sigma}_{\sigma\sigma'}^\alpha a_{Rj\sigma'}^\dagger a_{Lj\sigma'}(t_1)] \rangle, \\ \tilde{g}_{m,LR,ij}^r(t, t_1) = -i\theta(t - t_1) \\ \langle [\hat{\sigma}_{\sigma\sigma'}^\alpha a_{Li\sigma}^\dagger a_{Ri\sigma'}(t), \hat{\sigma}_{\sigma\sigma'}^\alpha a_{Lj\sigma'}^\dagger a_{Rj\sigma'}(t_1)] \rangle,$$

where $m = \alpha\alpha$, $\alpha = x, y, z$. The details are shown in Sec. A of the Supplemental Material [33].

With zero-bias voltage, we have only the DC Josephson current I^s generated by the tunneling of Cooper electron pairs through the Kitaev QSL. At $V \neq 0$, we are very interested in the DC current I^c and its conductance dI^c/dV of the normal single-particle tunneling. Thus the DC single-particle and Josephson current terms in the first-order approximation can be obtained as:

$$I^c = \frac{4e}{\hbar} \sum_{ij,m} \int \frac{d\epsilon}{2\pi} J_i J_j \text{Im} [\tilde{g}_{m,LR,ij}^r(eV - \epsilon)] \\ \text{Im} [g_{m,ij}^r(\epsilon)] [n(\epsilon) - n(\epsilon - eV)], \\ I^s = \frac{4e}{\hbar} \sum_{ij,m} \int \frac{d\epsilon}{2\pi} J_i J_j \text{Im} [\tilde{g}_{m,LR,ij}^r(\epsilon) g_{m,ji}^r(\epsilon)] \\ n(\epsilon) \sin \phi, \quad (5)$$

respectively, where $n(\epsilon) = 1/[\exp(\epsilon/k_B T) - 1]$ is the Bose-Einstein distribution function. As seen in Eq. (5), I^c clearly depends on the dynamical spin susceptibility $S_{ij}^m(\epsilon) = -2 \text{Im}[g_{m,ij}^r(\epsilon)]$ of the Kitaev QSL, the spectral weight of electron-hole modes $C_{LR,ij}^m(\epsilon) = -2 \text{Im}[\tilde{g}_{m,LR,ij}^r(\epsilon)]$ between the two SC leads, and the occupation difference between spins and electron-hole modes. Similarly, I^s is weighted by the hybridization spectrum of spins and Cooper pairs $A_{hy,ij}^m(\epsilon) = 2 \text{Im}[\tilde{g}_{m,LR,ij}^r(\epsilon) g_{m,ji}^r(\epsilon)]$ and the Bose-Einstein occupation $n(\epsilon)$. In these inelastic scattering processes, electron-hole modes or Cooper pairs with charge between the left and right SC leads transfer energy to the central spin system [25].

Further analysis reveals that both the normal and the anomalous Green's functions of the two leads have the same zz , xx , and yy components because of the time-reversal symmetry. We have $\tilde{g}_{m,LR,ij}^r(\epsilon) = \tilde{g}_{0,LR,ij}^r(\epsilon)$ and $\tilde{g}_{m,LR,ij}^r(\epsilon) = \tilde{g}_{0,LR,ij}^r(\epsilon)$ for $m = xx$ and yy , and zz , respectively. At the same time, due to the unique features of QSLs, $g_{m,ji}^r(\epsilon)$ is a short-range spin correlation in real space, and only the on-site and nearest-neighbor (NN) contributions are nonzero; this is explained later in Sec. II C. The currents have two-part contributions from the on-site and NN X , Y , and Z bonds. Therefore we can simplify the tunneling currents I^c and I^s at zero temperature as

$$I^c = \frac{8e}{\hbar} N J^2 \sum_m \int_0^{eV} \frac{d\epsilon}{2\pi} \left\{ \text{Im} [\tilde{g}_{0,LR,AA}^r(eV - \epsilon)] \text{Im} [g_{m,AA}^r(\epsilon)] \right. \\ \left. + \sum_{(AB)} \text{Im} [\tilde{g}_{0,LR,BA}^r(eV - \epsilon)] \text{Im} [g_{m,BA}^r(\epsilon)] \right\}, \\ I^s = \frac{8e}{\hbar} N J^2 \sum_m \int_0^\infty \frac{d\epsilon}{2\pi} \sin \phi \left\{ \text{Im} [\tilde{g}_{0,LR,AA}^r(\epsilon) g_{m,AA}^r(\epsilon)] \right. \\ \left. + \sum_{(AB)} \text{Im} [\tilde{g}_{0,LR,AB}^r(\epsilon) g_{m,BA}^r(\epsilon)] \right\}. \quad (6)$$

Here the indexes of the sublattices, AA and AB, stand for the on-site and NN configurations, respectively, and $J_i = J$ for each site i ; N is the number of unit cells in the honeycomb lattice.

The normal and anomalous two-body Green's functions can then be evaluated through frequency summations over the combinations of the left- and right-lead single-

body Green's functions in the 4×4 Nambu representation ($a_{nk\uparrow}^\dagger a_{n,-k\downarrow}^\dagger a_{nk\downarrow} a_{n,-k\uparrow}$). The details can be seen in Sec. B of the Supplemental Material [33]. We thus obtain that

$$\tilde{g}_{0,LR,AA(BA)}^r(\epsilon) = \frac{s^2}{2} \int \frac{d^2k}{4\pi^2} \int \frac{d^2p}{4\pi^2} e^{i(\mathbf{k}+\mathbf{p}) \cdot \mathbf{R}_{AA(BA)}} \left\{ \frac{1}{\epsilon - E_{Rp} - E_{Lk} + i0^+} - \frac{1}{\epsilon + E_{Rp} + E_{Lk} + i0^+} \right\}, \quad (7a)$$

$$\tilde{g}_{0,LR,AA(AB)}^r(\epsilon) = -\frac{s^2}{2} \int \frac{d^2k}{4\pi^2} \int \frac{d^2p}{4\pi^2} e^{i(\mathbf{k}+\mathbf{p}) \cdot \mathbf{R}_{AA(AB)}} \frac{\Delta_L \Delta_R}{E_{Lk} E_{Rp}} \left\{ \frac{1}{\epsilon - E_{Rp} - E_{Lk} + i0^+} - \frac{1}{\epsilon + E_{Rp} + E_{Lk} + i0^+} \right\}. \quad (7b)$$

Here $E_{nk(p)} = \sqrt{\epsilon_{nk(p)}^2 + \Delta_n^2}$, the parabolic energy dispersions $\epsilon_{Lk} = \hbar^2 k^2 / 2m^* - E_F$ and $\epsilon_{Rp} = \hbar^2 p^2 / 2m^* - E_F$, m^* is the effective electron mass, E_F is the Fermi energy level, we set $\hbar = 1$, s is the area of a unit cell of the SC–Kitaev layer–SC interface in the SC leads, and $R_{AA} = 0$ and $R_{AB} = X, Y, Z$ for the on-site and NN contributions, respectively.

We assume that $k_F = 1/a_s$ and $E_F = 20K$, where k_F and a_s are the Fermi wave vector and lattice constant of the two SC leads, respectively. Since the exchanged momenta between the SC leads and the Kitaev layer are constrained by $0 \leq |\mathbf{q}| \leq 2k_F$, the product $\mathbf{q} \cdot \mathbf{X}(Y, Z)$ ($\mathbf{q} = \mathbf{k} + \mathbf{p}$) can be taken as zero for simplicity [24,25] in the Green's functions with the NN contribution. This is suitable for “bad metals” such as Nb or Pb, which have small Fermi wave vectors. Hence in the leads, we have $\tilde{g}_{0,LR,AB(BA)}^r(\epsilon) \approx \tilde{g}_{0,LR,AA(BB)}^r(\epsilon)$ and $\tilde{g}_{0,LR,AB(BA)}^r(\epsilon) \approx \tilde{g}_{0,LR,AA(BB)}^r(\epsilon)$. The imaginary part of the normal retarded Green's function of the leads can then be further simplified as

$$\text{Im} [\tilde{g}_{0,LR,AA}^r(\epsilon)] = -2\pi \rho_L \rho_R \begin{cases} \int_{\Delta_L}^{\epsilon} dE \frac{E}{\sqrt{E^2 - \Delta_L^2}} \frac{(\epsilon - E)}{\sqrt{(\epsilon - E)^2 - \Delta_R^2}}, & \epsilon \geq E + \Delta_R \\ \int_{\Delta_L}^{-\epsilon} dE \frac{E}{\sqrt{E^2 - \Delta_L^2}} \frac{(\epsilon + E)}{\sqrt{(\epsilon + E)^2 - \Delta_R^2}}, & \epsilon \leq -E - \Delta_R \end{cases}, \quad (8a)$$

as well as the imaginary and real parts of the anomalous retarded Green's function

$$\begin{aligned} \text{Im} [\tilde{g}_{0,LR,AA}^r(\epsilon)] &= \frac{\pi}{2} \rho_L \rho_R \begin{cases} \int_{\Delta_L}^{\epsilon} dE \frac{\Delta_L}{\sqrt{E^2 - \Delta_L^2}} \frac{\Delta_R}{\sqrt{(\epsilon - E)^2 - \Delta_R^2}}, & \epsilon \geq E + \Delta_R \\ \int_{\Delta_L}^{-\epsilon} dE \frac{\Delta_L}{\sqrt{E^2 - \Delta_L^2}} \frac{-\Delta_R}{\sqrt{(\epsilon + E)^2 - \Delta_R^2}}, & \epsilon \leq -E - \Delta_R \end{cases}, \\ \text{Re} [\tilde{g}_{0,LR,AA}^r(\epsilon)] &= \int_{-\infty}^{\infty} \frac{d\omega}{2\pi} \frac{(-2) \text{Im} [\tilde{g}_{0,LR,AA(AB)}^r(\omega)]}{\epsilon - \omega}. \end{aligned} \quad (8b)$$

Here we calculate the real part of the Green's function by using the Kramers–Kronig transformation. The normal density of states (DOS) in the 2D interface $\rho_{L(R)} = m^* a_s^2 / 2\pi \hbar^2$. More details can be seen in Sec. B of the Supplemental Material [33].

We can thus obtain the DC single-particle differential conductance dI^c/dV and the derivative of the DC Josephson current I^s with respect to Δ , $dI^s/d\Delta$ as

$$\begin{aligned} \frac{dI^c}{dV} &= \frac{2e^2}{\hbar} NJ^2 \sum_m \int_0^{eV} \frac{d\epsilon}{2\pi} \left\{ \frac{d[C_{LR,AA}^0(eV - \epsilon)]}{dV} S^m(\epsilon) \right\}, \\ \frac{dI^s}{d\Delta} &= \frac{4e}{\hbar} NJ^2 \sum_m \int_0^{\infty} \frac{d\epsilon}{2\pi} \frac{d[A_{hy}^m(\epsilon)]}{d\Delta} \sin \phi. \end{aligned} \quad (9)$$

Here the total dynamical spin susceptibility, the total hybridization spectrum of spins and Cooper pairs, and the equally weighted spectrum of electron–hole modes are defined as

$$\begin{aligned} S^m(\epsilon) &= -2 \text{Im} [g_m^r(\epsilon)], \\ A_{hy}^m(\epsilon) &= 2 \text{Im} \{ \tilde{g}_{0,LR,AA}^r(\epsilon) g_m^r(\epsilon) \}, \\ C_{LR,AA}^0(\epsilon) &= -2 \text{Im} [\tilde{g}_{0,LR,AA}^r(\epsilon)], \end{aligned} \quad (10)$$

respectively, where the total Green's function of spin correlation $g_m^r(\epsilon) = g_{m,AA}^r(\epsilon) + \Sigma_{(AB)} g_{m,BA}^r(\epsilon)$. Once the Green's functions $\tilde{g}_{0,LR,AA}^r(\epsilon)$, $\tilde{g}_{0,LR,AA}^r(\epsilon)$, and $g_m^r(\epsilon)$ have been obtained, we can find the DC single-particle current and its differential conductance numerically, as well as the zero-voltage Josephson current at zero temperature.

C. Dynamics of the Kitaev model

Next, we need the total Green's function of the spin correlation of the anisotropic Kitaev QSL, $g_m^r(\epsilon)$, whose imaginary part corresponds to the dynamical spin susceptibility, $S^m(\epsilon)$. We can evaluate $S^m(\epsilon)$ by employing the few-particle-response method and $g_m^r(\epsilon)$ via the Kramers–Kronig transformation.

The Kitaev model H_{cen} in Eq. (1) can be exactly solved by introducing four Majorana fermions b_i^α ($\alpha = x, y, z$) and c_i per site for the local spins, i.e., $\hat{\sigma}_i^\alpha = ic_i b_i^\alpha$. We define the bond operators $\hat{u}_{ij}^\alpha = ib_i^\alpha b_j^\alpha$ on the NN bond $\langle ij \rangle_\Lambda$ ($\Lambda = X, Y, Z$), respectively. Their eigenvalues are $u_{ij}^\alpha = \pm 1$, and they commute with H_{cen} and with each other. The Kitaev model can therefore be expressed in terms of the different sets of $\{u_{ij}^\alpha\}$ and the Majorana fermions [8,32],

$$H_{\text{cen}} = i \sum_{\Lambda, \langle ij \rangle_\Lambda} K_\Lambda u_{ij}^\alpha c_i c_j, \quad (11)$$

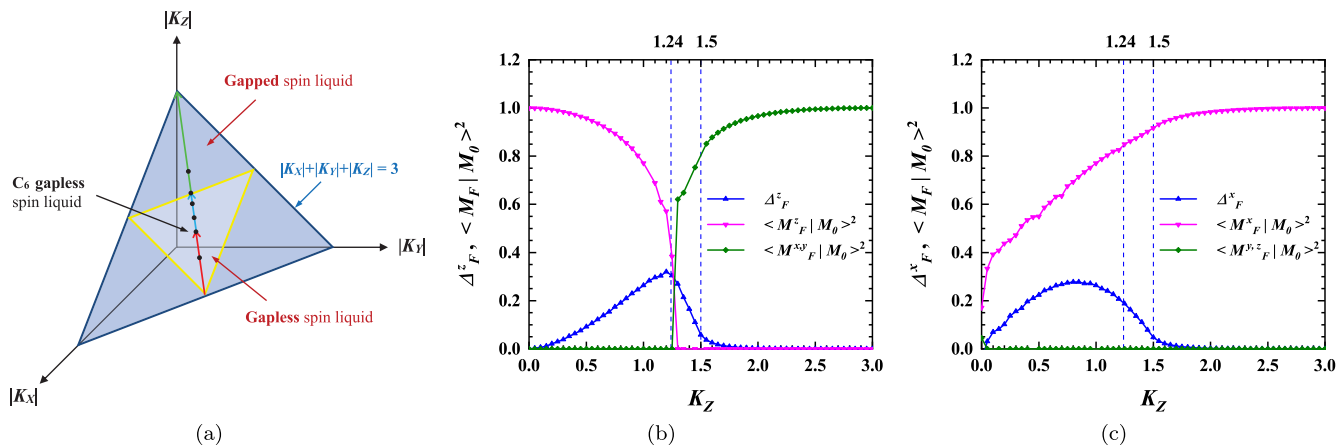


FIG. 3. (a) Variation range of Kitaev coupling strengths in the parametric phase diagram of the Kitaev model with the conditions $K_X = K_Y$ and $K_X + K_Y + K_Z = 3.0$ marked by red, blue, and green arrows. Six points are marked with black dots, $K_Z = 1.8, 1.5, 1.4, 1.24, 1.0,$ and 0.6 . Kitaev coupling K_Z dependences of (b) the overlaps $\langle M_F^z | M_0 \rangle^2$, $\langle M_F^{x,y} | M_0 \rangle^2$, and vison gap Δ_F^z , and (c) the overlaps $\langle M_F^x | M_0 \rangle^2$, $\langle M_F^{y,z} | M_0 \rangle^2$, and vison gap Δ_F^x in the variation range of panel (a).

where the product of all bond operators around a plaquette, $W_p = \prod_{i,j \in p} u_{ij}^{\alpha} \doteq \pm 1$, can define the flux sectors. The eigenstates of this model are Z_2 gauge fluxes threading the plaquettes and Majorana fermions (or spinons) propagating between sites in this Z_2 gauge field [32]. Their wave vectors $|\Phi\rangle$ are the direct product of the bond (gauge flux) and Majorana-matter-fermion degrees of freedom, $|\Phi\rangle = |F\rangle \otimes |M\rangle$. The ground state is within the zero-flux sector, with $W_p = 1$ ($u_{ij}^{\alpha} = 1$) for all plaquettes.

Through the diagonalization of the zero-flux Hamiltonian matrix in momentum space, the ground-state spinon energy dispersion can be expressed as

$$E_{\mathbf{k}} = 2|K_X e^{i\mathbf{k} \cdot \mathbf{X}} + K_Y e^{i\mathbf{k} \cdot \mathbf{Y}} + K_Z e^{i\mathbf{k} \cdot \mathbf{Z}}|. \quad (12)$$

The ground-state parametric phase diagram can then be obtained [8], as shown in Fig. 3(a). From Eq. (12), one can find a van Hove singularity at $E_{V1} = 2|K_Z|$ corresponding to the energy contour line PMP' in the first Brillouin region, and there is another van Hove singularity at $E_{V2} = 2|K_X + K_Y - K_Z|$ when $|K_Z| < 1.5$, or a spinon gap $\Delta_S = 2|K_Z - K_X - K_Y|$ when $1.5 < |K_Z| < 3.0$, associated with the M' point. There is also an energy maximum $E_{\max} = 2|K_X + K_Y + K_Z| = 6$ at the Γ point. In probing into the dynamical features and evolution of the QSL ground states in the anisotropic Kitaev model, we take the range of the Kitaev couplings K_Z along the red, blue, and green lines with arrows, indicating a gapped, gapless, and another gapless QSL, in this phase diagram. The quantum phases in these three regions display distinctly different quantum features [30].

The time-dependent dynamical spin susceptibility of the ground state, $S_{ij}^{\alpha\alpha}(t) = 0.25 \langle \Phi_0 | \hat{\sigma}_i^{\alpha}(t) \hat{\sigma}_j^{\alpha}(0) | \Phi_0 \rangle$ ($|\Phi_0\rangle = |F_0\rangle \otimes |M_0\rangle$) [32], can be derived as follows:

$$S_{ij}^{\alpha\alpha}(t) = -0.25i \langle M_0 | e^{iH_0 t} c_i e^{-i(H_0 + V_{(ij)\Lambda})t} c_j | M_0 \rangle \times (i\delta_{ij} + \hat{u}_{ij}^{\alpha} \delta_{(ij),\Lambda}), \quad (13)$$

where $V_{(ij)\Lambda} = -2iK_{\Lambda} c_i c_j$, $i \in A$, $j \in B$, and $\alpha = x, y, z$ has a one-to-one correspondence with $\Lambda = X, Y, Z$. We can find that only the on-site (δ_{ij}) and NN ($\delta_{(ij),\Lambda}$) contributions to the

dynamical spin correlations are nonzero, and $S_{ij}^{\alpha\alpha}$ only has the $\alpha = z(x, y)$ component in the NN $X(Y, Z)$ bond.

$S_{ij}^{\alpha\alpha}$ can have the Lehmann representation by inserting the identity $\mathbf{1} = \sum_{\lambda} |\lambda\rangle \langle \lambda|$ of the two-flux sector with a flipping bond $u_{ij}^{\alpha} = -1$. The main contributions are from the zero-, one-, and two-particle components of $|\lambda\rangle$, which occupy 98% of the total [32]. We can thus obtain the dynamical spectrums in frequency (ω) space as

$$S_{AA}^{\alpha\alpha}(\omega) = \frac{\pi}{2} \sum_{\lambda} \langle M_0 | c_A |\lambda\rangle \langle \lambda | c_A | M_0 \rangle \delta[\omega - (E_{\lambda}^F - E_0)],$$

$$S_{BA}^{\alpha\alpha}(\omega) = \frac{\pi}{2} i \sum_{\lambda} \langle M_0 | c_B |\lambda\rangle \langle \lambda | c_A | M_0 \rangle \delta[\omega - (E_{\lambda}^F - E_0)]. \quad (14)$$

Here E_0 is the ground-state energy of the zero-flux sector, E_{λ}^F is the energy eigenvalue of state $|\lambda\rangle$ of the two-flux sector [32], the lowest energy is E_0^F with the state $|M_F^{z(x,y)}\rangle$, and E_{λ}^F are obtained through diagonalization of the two-flux Hamiltonian matrix in real space. We can calculate the overlaps $\langle M_0 | M_F^{z(x,y)} \rangle^2$ and the ‘‘vison’’ gap $\Delta_F^{z(x,y)} = E_0^F - E_0$ due to the gauge-flux excitation, as shown in Figs. 3(b) and 3(c); this is consistent with Knolle’s results [32].

From the dynamical phase diagrams in Figs. 3(b) and 3(c), we can see that the lowest-energy states of the zero-flux sector H_0 and two-flux sector $H_0 + V_{z(x,y)}$, i.e., $|M_0\rangle$ and $|M_F^{z(x,y)}\rangle$, conserve the parity owing to the spatial inversion symmetry. Along the line in Fig. 3(a), $|M_0\rangle$ and $|M_F^z\rangle$ have the same parity when $0 < |K_Z| < 1.24$ and the opposite parity when $1.24 < |K_Z| < 3.0$; $|M_0\rangle$ and $|M_F^{x(y)}\rangle$ have the same parity throughout. In the case with the same parity, $|\lambda\rangle$ must have an odd number of excitations, and these are mainly the single-particle contributions [32]. These dynamical spin susceptibilities can be evaluated by using Eq. (12). In the opposite case, $|\lambda\rangle$ only contain an even number of excitations, and these are mainly the zero- and two-particle contributions [32]. The Lehmann representation is actually modified by inserting the identity $\mathbf{1} = \sum_{\lambda} c_{A(B)} |\lambda\rangle \langle \lambda | c_{A(B)}$ of two-flux sector $H_0 + V_x + V_y$

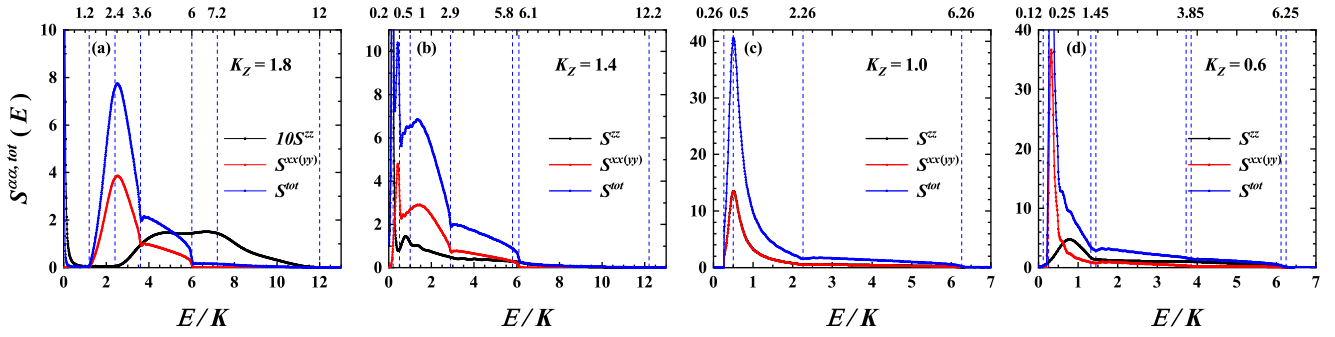


FIG. 4. Energy (E) dependences of the dynamical spin susceptibilities of the anisotropic Kitaev QSL, including the total S^{tot} and its three components $S^{\alpha\alpha}(E)$ ($\alpha = x, y, z$) for different Kitaev couplings (in units of K): $K_Z =$ (a) 1.8; (b) 1.4; (c) 1.0; (d) 0.6. Here $S^{\text{xx}} = S^{\text{yy}}$.

with two flipping bonds $u_{ij}^x, u_{ij}^y = -1$. Its lowest-energy state $|M_F^{x,y}\rangle$ has the same parity as $|M_0\rangle$ [32], as shown in Fig. 3(b). We also plot the lowest-energy state $|M_F^{y,z}\rangle$ for $H_0 + V_y + V_z$, as shown in Fig. 3(c). This has the opposite parity to $|M_0\rangle$ throughout. Therefore we can explicitly express Eq. (11) for the zero- and two-particle contributions:

$$S_{AA}^{\alpha\alpha}(\omega) = \frac{\pi}{2} \sum_{\lambda} \langle M_0 | \lambda \rangle \langle \lambda | M_0 \rangle \delta[\omega - (E_{\lambda}^F - E_0)],$$

$$S_{BA}^{\alpha\alpha}(\omega) = \frac{\pi}{2} i \sum_{\lambda} \langle M_0 | c_{BCA} | \lambda \rangle \langle \lambda | M_0 \rangle \delta[\omega - (E_{\lambda}^F - E_0)].$$
(15)

The dynamical spin correlation is then $S^m(\epsilon) = S_{AA}^m(\epsilon) + S_{BA}^m(\epsilon)$ ($m = \alpha\alpha, \alpha = x, y, z$). More details are given in Sec. C of the Supplemental Material [33]. Hence combining the dynamical and parametric phase diagrams, we choose four representative points $K_Z = 1.8, 1.4, 1.0$, and 0.6 , respectively, among the phase-transition points about the parity relationship and spinon gap, $K_Z = 1.24$ and 1.5 .

Substituting Eqs. (8), (14), and (15) into Eqs. (6), (9), and (10), we can obtain the tunneling current $I^{c,s}$ and differential conductances dI^c/dV and $dI^s/d\Delta$. Throughout this paper, the SC order parameters $\tilde{\Delta}_L$ and $\tilde{\Delta}_R$ in the left and right leads have the same modulus $\Delta_L = \Delta_R = \Delta$ but different phases $\phi_{L(R)}$. All of the energies are measured in terms of the Kitaev coupling K , which can be taken as $K = 1$.

III. RESULTS AND DISCUSSION

A. Dynamical spin correlations of the anisotropic Kitaev model

First, we plot the dynamical spin susceptibilities of the anisotropic Kitaev model, including the components $S^{\alpha\alpha}(E)$ ($\alpha = x, y, z$) and their total S^{tot} as functions of energy E [24–26,31,32], as shown in Figs. 4(a)–4(d). Here $S^{\text{xx}} = S^{\text{yy}}$ because $K_X = K_Y$. We can see that the anisotropic components of dynamical spin susceptibilities [S^{zz} and $S^{\text{xx(yy)}}$] and their total (S^{tot}) reveal remarkably different features in these four quantum phases.

When $K_Z = 1.8$ with a gapped QSL, the parities between $|M_F^z\rangle$ and $|M_0\rangle$ are opposite. As shown in Fig. 4(a), in $S^{\text{xx(yy)}}$ we can see the total QSL gap $\Delta_t \approx 1.2$. This actually contains the spinon gap $\Delta_S = 2|K_Z - K_X - K_Y| = 1.2$ and vison gap $\Delta_F^x \approx 0.0$. There is a dip at $E \approx 3.6$ owing to the van Hove

singularity of the spinon spectrum at $2K_Z$ and an energy shift of Δ_F^x . An upper edge also emerges at about 6.0, which is equal to $\Delta_F^x + 2|K_X + K_Y + K_Z|$. These three feature points in $S^{\text{xx(yy)}}$ thus have a one-to-one correspondence with those of spinon dispersion at E_V (Δ_S or E_{V1}, E_{V2} , and E_{max}), and they move toward $\Delta_F^{x(y)} + E_V$. There is a new peak at about 2.5 caused by vison–spinon interactions. However, in S^{zz} , we can observe the total gap $\Delta_t' \approx 2.4$, which stems from $\Delta_F^z \approx 0.0$ and the new spinon gap $\Delta_S' = 2\Delta_S$. A peak appears at $E \approx 7.2$ resulting from the van Hove singularity, and the upper edge emerges at $E \approx 12.0$. The three feature points at $\Delta_F^z + 2E_V$ in S^{zz} are from the virtual transitions to the eigenstates of the two-flux sector with two flipping bonds. Moreover, we can see a distinct sharp peak at Δ_F^z , which stems from the virtual transitions to the lowest-energy state, $|M_F^{x,y}\rangle$. There is also a new peak around 5.0 due to vison–spinon interactions. Note that $S^{\text{xx(yy)}}$ is an order of magnitude larger than S^{zz} . As for the sum of $S^{\text{zz}}, S^{\text{xx}},$ and $S^{\text{yy}}, S^{\text{tot}}$ can provide complete information about visons, spinons, and their interactions apart from some feature points because of the resolution of S^{zz} .

When $K_Z = 1.4$, as shown in Fig. 4(b), the ground state is gapless QSL, and $|M_F^z\rangle$ and $|M_0\rangle$ have opposite parity. Hence the three feature points are displayed on $S^{\text{xx(yy)}}$ and S^{zz} in a similar way as for $K_Z = 1.8$ except for the van Hove singularity rather than the spinon gap. In S^{xx} , we can observe two dips at $E \approx 0.5$ and 2.9 corresponding to the van Hove singularities, and there is an upper edge at about 6.1, with $\Delta_F^x \approx 0.11$. These three feature points emerge at $\Delta_F^{x(y)} + E_V$. There are two new interaction peaks at about 0.4 and 1.5. In S^{zz} , there is a dip and an inflection point associated with the van Hove singularities at $E \approx 1.0$ and 5.8 , and there is a boundary at about 12.2, with $\Delta_F^z \approx 0.17$. These feature points are therefore shown at $\Delta_F^z + 2E_V$. A remarkable sharp peak appears at Δ_F^z , and a new interaction peak emerges at about 0.8. Since S^{zz} has the same order of magnitude as $S^{\text{xx,yy}}, S^{\text{tot}}$ can also reveal the full dynamical features of the Kitaev QSL.

When $K_Z = 1.0$ and 0.6 , as shown in Figs. 4(c) and 4(d), $|M_F^{z(x,y)}\rangle$ and $|M_0\rangle$ have the same parity. At $K_Z = 1.0$, the ground state of the isotropic Kitaev model is a C_6 gapless QSL, and the $S^{\text{xx(yy)}}$ and S^{zz} components are equal, $\Delta_F^{x(y)} = \Delta_F^z \approx 0.26$. From S^{zz} , we can find that there is only one dip related to the two-in-one van Hove singularity at $E \approx 2.26$, and there is an upper edge at about 6.26. There is also a new interaction peak at about 0.5. At $K_Z = 0.6$, two dips resulting

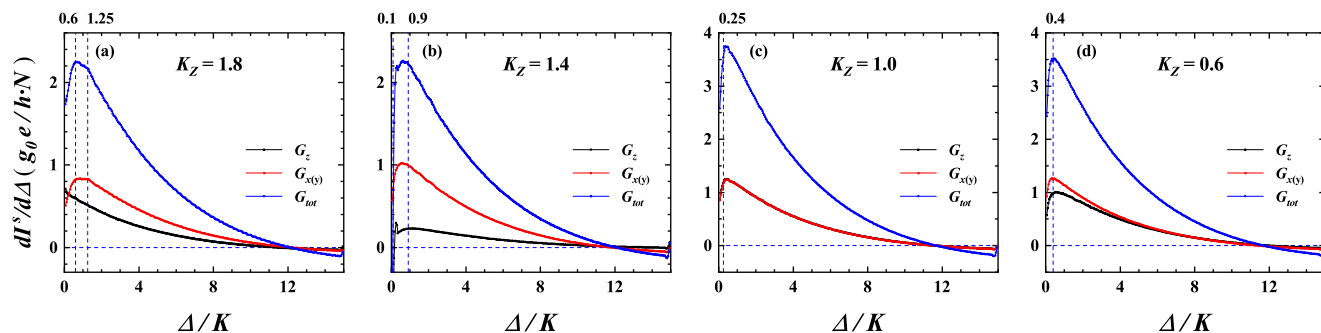


FIG. 5. Derivatives of the DC Josephson tunneling current I^s with respect to the SC gap, $dI^s/d\Delta$, including the components $G_{z(x,y)}$ ($G_x = G_y$) and G_{tot} as functions of the SC gap Δ for different Kitaev couplings (in units of K): $K_Z =$ (a) 1.8; (b) 1.4; (c) 1.0; (d) 0.6. Here $\phi = 3\pi/2$.

from the van Hove singularities, an upper edge, and a new sharp peak are shown at $E \approx 1.45, 3.85, 6.25$, and 0.3 in $S^{xx(yy)}$ with $\Delta_F^{x(y)} \approx 0.25$. There is a dip, an inflection point, an upper boundary, and a new peak at $E \approx 1.32, 3.72, 6.12$, and 0.8 in S^{zz} with $\Delta_F^z \approx 0.12$. Therefore feature points emerge at $\Delta_F^{x(y)} + E_V$ and $\Delta_F^z + E_V$ in $S^{xx(yy)}$ and S^{zz} , respectively, because of the virtual transitions to the eigenstates of the two-flux sector with only a flipping $X(Y)$ or Z bond. The total spin correlations S^{tot} also contain the entire characters of the Kitaev QSL when $K_Z = 1.0$ and 0.6 .

In summary, the dynamical spin susceptibility components S^{zz} and $S^{xx} (= S^{yy})$ reveal different vison gaps Δ_F^z and $\Delta_F^{x(y)}$, respectively. Each component can only reveal partial features of the Majorana fermion (spinon) dispersions influenced by the gauge fluxes, including the two van Hove singularities (or a spinon gap and a van Hove singularity) and the energy upper edge, and in different ways. Therefore S^{tot} can reveal the complete information about the Kitaev QSL well. There are some new peaks between these feature points, and these stem from the interactions between the vison and the spinon excitations.

B. DC Josephson current with zero voltage

In the absence of a bias voltage, only the DC Josephson current with the tunneling of the Cooper pairs is presented in the SC–Kitaev QSL–SC junction. The SC gap Δ dependences of the derivative of the DC Josephson current I^s with respect to Δ , $G_{tot} = dI^s/d\Delta$, and its components $G_{z(x,y)}$ ($G_x = G_y$) are shown in Figs. 5(a)–5(d) for different Kitaev couplings $K_Z = 1.8, 1.4, 1.0$, and 0.6 , respectively. Here the phase difference $\phi = 3\pi/2$, and we define the dimensionless constant $g_0 = 4\pi \rho_L \rho_R J^2$.

As can be seen in Figs. 5(a)–5(d), when $K_Z = 1.8$, there is a peak at $\Delta \approx 0.6$ and an inflection point at about 1.25 . The former corresponds to the total QSL gap $\Delta_t \approx 1.2$, which originates from the resonant tunneling when $2\Delta = \Delta_t$, while the latter stems from interactions between vison and spinon excitations near $2\Delta \approx 2.5$. Similarly, at $K_Z = 1.4$, a distinct peak, corresponding to the total QSL gap, emerges around $2\Delta \approx 0.17$. Another peak at about 0.9 stemming from the response to the interaction peak appears near $2\Delta \approx 1.8$. When $K_Z = 1.0$ and 0.6 , we can only observe the peaks at about 0.25 and 0.4 , which is due to the response to the interaction

peaks around $2\Delta \approx 0.5$ and 0.8 , respectively. Thus $dI^s/d\Delta$ curves mainly provide information about the interaction of gauge fluxes and Majorana fermion modes, as well as the total QSL gap. These peaks in $dI^s/d\Delta$ can be seen from the dynamical spin susceptibilities in Fig. 4; however, they only provide partial information about the Kitaev QSLs.

To understand this, the energy (E) dependences of the total dynamical hybridization spectral functions between the local spins of the Kitaev layer and the Cooper pairs of the two SC leads, $A_{hy} = \sum_{\alpha} A_{hy}^{\alpha\alpha}$ ($\alpha = x, y, z$), are plotted in Figs. 6(a)–6(d), in which the SC gaps are set as $\Delta = 1, 3$, and 5 . We can clearly see the complete dynamical spin correlation characters, and $A_{hy} > 0$ before $E = 2\Delta$. When $E > 2\Delta$, these spin-correlation features appear with a reversed sign, i.e., $A_{hy} < 0$ in the same magnitude. Thus the DC Josephson current at zero bias, as the frequency integration of the hybridization spectrum, is partially canceled; hence it only retains partial information about the Kitaev QSL. This arises from the fact that, in inelastic tunneling, the quasielectrons and quasiholes of the SC Cooper pairs contribute to the positive and negative parts of A_{hy} , respectively. Therefore the total response to the dynamical spin-correlation spectrum is canceled out due to the spin-singlet Cooper pairs.

C. DC conductance of normal single-particle tunneling

In the presence of a DC bias voltage in the SC–Kitaev QSL–SC junction, one can reveal more characters of the Kitaev QSL. The bias potential eV dependences of the DC single-particle differential conductance $G_{tot} = dI^c/dV$, as well as its $zz(xx, yy)$ components $G_{z(x,y)}$, are described in Figs. 7(a)–7(d) for different Kitaev couplings $K_Z = 1.8, 1.4, 1.0$, and 0.6 , respectively. Here we define the conductance constant $G_0 = g_0 e^2/h$, and $G_{tot} = G_x + G_y + G_z$, with $G_x = G_y$.

From Figs. 7(a)–7(d), it can be seen that the single-particle DC differential conductance spectrums of the SC junction, G_{tot} and $G_{z(x,y)}$, show distinctly different characters in the four quantum phases. To clearly see the dynamical behaviors of G_{tot} in the present anisotropic Kitaev layer, we first describe the bias voltage dependence of $G_{z(x,y)}$. When $K_Z = 1.8$, as seen in Fig. 7(a), in contrast with the dynamical spin susceptibility in Fig. 4(a), the threshold of the conductance $G_{x(y)}$ is modulated up to about 3.2 , i.e., $\Delta_t + 2\Delta$. This arises from the

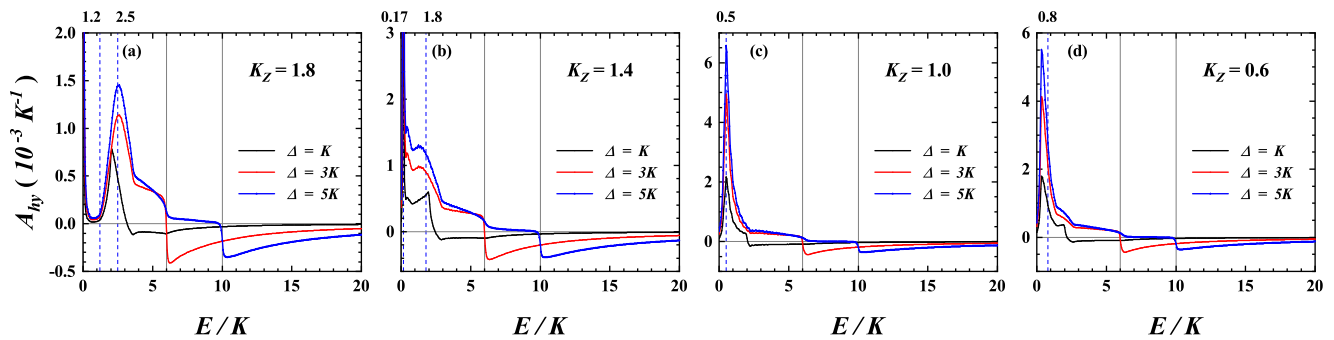


FIG. 6. Energy (E) dependences of the total hybridization spectral functions between spins of the central Kitaev QSL layer and Cooper pairs of the two SC leads, A_{hy} , with $\Delta = 1, 3$, and 5 for different Kitaev couplings (in units of K): $K_Z =$ (a) 1.8 ; (b) 1.4 ; (c) 1.0 ; (d) 0.6 .

fact that the electrons at the bottom of the SC gap in the right lead need a high enough bias potential $eV = \Delta + \Delta + \Delta_t$ to overcome the right and left SC gaps and the total QSL gap of the central layer along the X (Y) bond, and finally reach the empty state on the top of the SC gap in the left lead.

When $eV > 2\Delta + \Delta_t$, with the opening of the channel of the Majorana bound state, the conductance $G_{x(y)}$ starts to rise rapidly and goes up to a sharp peak at about 4.5 . This peak corresponds to the interaction peak of the dynamical spin correlation around 2.5 shown in Fig. 4(a), and it results from the dynamical creation of the Majorana fermions (or spinons) interacting with the two NN gauge fluxes in the virtual transition. Soon after this, a remarkable dip is observed at about 5.6 , which is associated with the dip of the dynamical spectrum around 3.6 and is due to the van Hove singularities of the DOS of the Majorana dispersive band. Finally, the single-particle conductance approaches a constant after the upper edge at about 8 due to the edge of the Majorana dispersive bands around 6 . The features of the single-particle DC differential conductance spectrums $G_{x(y)}$ in Fig. 7(a) thus have a one-to-one correspondence with those of the dynamical spin susceptibility in Fig. 4(a).

We can also see a remarkable sharp peak at $eV \approx 2$ in G_z that is related to the peak in the dynamical spectrum near $\Delta_z^F \approx 0.0$. This originates from the δ -function contribution of the virtual transition between the ground state $|M_0\rangle$ and the excited state $|M_F^{x,y}\rangle$. When $eV > \Delta_z^F$, no obvious characters in G_z are observed since S^{zz} is an order of magnitude smaller than $S^{xx(yy)}$. Summing the three components gives rise

to the total conductance G_{tot} , which contains the complete characters of the spinon spectrums, vison excitations, and their interactions in the Kitaev QSL. Thus compared with a normal-metal junction situation [24,25], the present differential conductance spectrums G_{tot} have a more intuitive and sensitive response to the characters of the dynamical spin correlation components of the Kitaev QSL, S^{tot} .

When $K_Z = 1.4, 1.0$, and 0.6 , similar to $K_Z = 1.8$, the single-particle DC differential conductance spectrums $G_{z(x,y)}$ are able to reflect the features of the dynamical spin susceptibility components $S^{zz(xx,yy)}$ well, aside from some feature points due to the resolution of the numerical integration. Fortunately, in the present situations with $K_Z = 1.4, 1.0$, and 0.6 , the z components of the dynamical spin correlations S^{zz} are the same order of magnitude as $S^{xx,yy}$, so G_z can resolve all of the features of S^{zz} . Hence from the single-particle tunneling spectrums, we can obtain insights into the features of the dynamical spin susceptibilities of the Kitaev QSL.

IV. CONCLUSION

In our present theory, we point out two possible improvements to previous results. On the one hand, with the condition $\mathbf{q} \cdot \mathbf{X}(\mathbf{Y}, \mathbf{Z}) \approx 0$, we obtain the features of the total dynamical spin susceptibility S^{tot} . When $\mathbf{q} \cdot \mathbf{X}(\mathbf{Y}, \mathbf{Z}) \neq 0$, the individual contributions of each component of the NN spin correlation $S_{BA}^{\alpha\alpha}$ to the tunneling currents would be slightly different from the results above. Our further study reveals that, in this situation, the correction to Eq. (8) only quantitatively alters

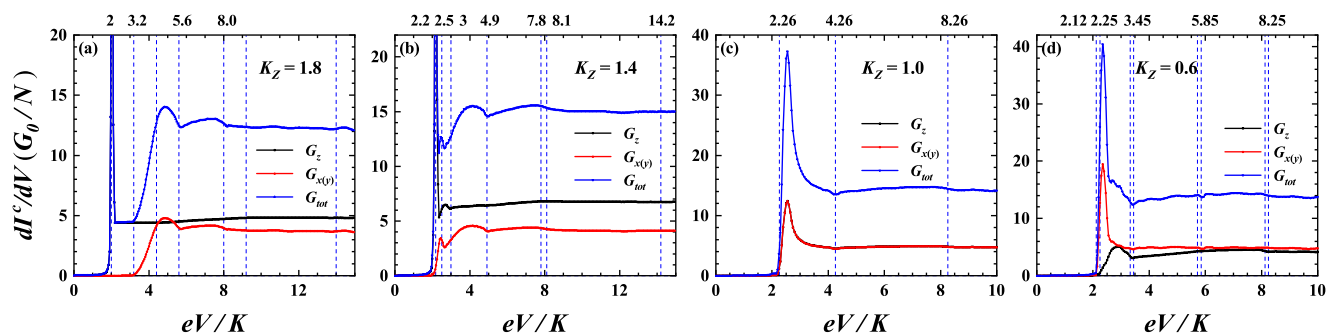


FIG. 7. DC differential conductances of single-particle tunneling dI/dV , including the components $G_{z(x,y)}$ ($G_x = G_y$) and G_{tot} as functions of the bias potential eV for different Kitaev couplings (in units of K): $K_Z =$ (a) 1.8 ; (b) 1.4 ; (c) 1.0 ; (d) 0.6 .

the tunneling current; nevertheless, it is qualitatively consistent with the above conclusion. On the other hand, although the zero-voltage Josephson current fails to measure the full information about the Kitaev QSL in the elastic scattering process, we expect that the AC Josephson currents with a DC bias voltage will reveal more features of the dynamical spin correlation, which goes beyond the scope of this paper.

In summary, in investigating the electron tunneling transport and its spectroscopic features in an SC–anisotropic Kitaev QSL–SC Josephson junction with a weak link, we assume that inelastic scattering tunneling of single particles and Cooper pairs is realized by the s – d exchange interaction. As expected, the DC differential conductance dI^c/dV of the normal single-particle tunneling succeeds in exhibiting the dynamical spin susceptibility characters of the anisotropic Kitaev QSL—including unique spin gaps (even in gapless QSL), sharp or broad peaks, small dips, and the upper edge of the itinerant Majorana fermion dynamics—except for the energy shift of the two-SC-lead gap 2Δ . The different topological quantum phases of the anisotropic Kitaev QSL can be

distinguished well by using the tunneling spectral features. Unusually, the zero-voltage DC Josephson currents I^s only contain some residual information about the Kitaev QSL, which stems from the spin singlets of Cooper pairs.

Our results may pave a new path to measurement of the Majorana–fermion dynamical correlation features of anisotropic Kitaev and other spin-liquid materials. We expect that our theoretical results will be confirmed by future experiments and applied to SC junction devices.

ACKNOWLEDGMENTS

L.-J.Z. thanks the supports from the National Natural Science Foundation of China under Grants No. 11774350 and No. 11474287, H.-Q.L. acknowledges financial support from NSAF U1930402 and NSFC 11734002. X.-L.Y. thanks the support from the Science, Technology, and Innovation Commission of Shenzhen Municipality of China under Grant No. JCYJ20190809120203655. Numerical calculations were performed at the Center for Computational Science of CASHIPS and Tianhe II of CSRC.

-
- [1] L. Balents, Spin liquids in frustrated magnets, *Nature (London)* **464**, 199 (2010).
- [2] Z. Y. Meng, T. C. Lang, S. Wessel, F. F. Assaad, and A. Muramatsu, Quantum spin liquid emerging in two-dimensional correlated dirac fermions, *Nature (London)* **464**, 847 (2010).
- [3] P. W. Anderson, Resonating valence bonds: A new kind of insulator?, *Mater. Res. Bull.* **8**, 153 (1973).
- [4] P. Fazekas and P. W. Anderson, On the ground state properties of the anisotropic triangular antiferromagnet, *Philos. Mag.* **30**, 423 (1974).
- [5] F. Mezzacapo and M. Boninsegni, Ground-state phase diagram of the quantum J_1 – J_2 model on the honeycomb lattice, *Phys. Rev. B* **85**, 060402(R) (2012).
- [6] X.-L. Yu, D.-Y. Liu, P. Li, and L.-J. Zou, Ground-state and finite-temperature properties of spin liquid phase in the J_1 – J_2 honeycomb model, *Physica E* **59**, 41 (2014).
- [7] G. Jackeli and G. Khaliullin, Mott Insulators in the Strong Spin-Orbit Coupling Limit: From Heisenberg To a Quantum Compass and Kitaev Models, *Phys. Rev. Lett.* **102**, 017205 (2009).
- [8] A. Kitaev, Anyons in an exactly solved model and beyond, *Ann. Phys.* **321**, 2 (2006).
- [9] A. Kitaev, Fault-tolerant quantum computation by anyons, *Ann. Phys.* **303**, 2 (2003).
- [10] N. Read and B. Chakraborty, Statistics of the excitations of the resonating-valence-bond state, *Phys. Rev. B* **40**, 7133 (1989).
- [11] S. S. Hegde, G. Yue, Y. X. Wang, E. Huemiller, D. J. Van Harlingen, and S. Vishveshwara, A topological josephson junction platform for creating, manipulating, and braiding majorana bound states, *Ann. Phys.* **423**, 168326 (2020).
- [12] S. V. Bakurskiy, A. A. Golubov, and M. Y. Kupriyanov, *Fundamentals and Frontiers of the Josephson Effect* (Springer-Verlag, Napoli, Italy, 2019).
- [13] T. Xiang, *D-Wave Superconductivity* (Science and Education Press, Beijing, China, 2007).
- [14] A. W. Kleinsasser, R. E. Miller, W. H. Mallison, and G. B. Arnold, Observation of Multiple Andreev Reflections in Superconducting Tunnel Junctions, *Phys. Rev. Lett.* **72**, 1738 (1994).
- [15] A. F. Morpurgo, B. J. van Wees, T. M. Klapwijk, and G. Borghs, Energy Spectroscopy of Andreev Levels Between Two Superconductors, *Phys. Rev. Lett.* **79**, 4010 (1997).
- [16] Q.-F. Sun, B.-G. Wang, J. Wang, and T.-H. Lin, Electron transport through a mesoscopic hybrid multiterminal resonant-tunneling system, *Phys. Rev. B* **61**, 4754 (2000).
- [17] Y. Zhu, Q.-F. Sun, and T.-H. Lin, Andreev reflection through a quantum dot coupled with two ferromagnets and a superconductor, *Phys. Rev. B* **65**, 024516 (2001).
- [18] Q.-F. Sun, H. Guo, and J. Wang, Hamiltonian approach to the ac josephson effect in superconducting-normal hybrid systems, *Phys. Rev. B* **65**, 075315 (2002).
- [19] E. A. Demler, G. B. Arnold, and M. R. Beasley, Superconducting proximity effects in magnetic metals, *Phys. Rev. B* **55**, 15174 (1997).
- [20] V. V. Ryazanov, V. A. Oboznov, A. Y. Rusanov, A. V. Veretennikov, A. A. Golubov, and J. Aarts, Coupling of Two Superconductors Through a Ferromagnet: Evidence for a π Junction, *Phys. Rev. Lett.* **86**, 2427 (2001).
- [21] E. C. Gingrich, B. M. Niedzielski, J. A. Glick, Y. X. Wang, D. L. Miller, R. Loloee, W. P. Pratt, Jr, and N. O. Birge, Controllable 0 – π Josephson junctions containing a ferromagnetic spin valve, *Nat. Phys.* **12**, 564 (2016).
- [22] L. P. Gor'kov and V. Z. Kresin, Josephson junction with an antiferromagnetic barrier, *Physica C: Superconduct.* **367**, 103 (2002).
- [23] L. Bulaevskii, R. Eneias, and A. Ferraz, Superconductor-antiferromagnet-superconductor π Josephson junction based on an antiferromagnetic barrier, *Phys. Rev. B* **95**, 104513 (2017).
- [24] M. Carrega, I. J. Vera-Marun, and A. Principi, Tunneling spectroscopy as a probe of fractionalization in two-dimensional magnetic heterostructures, *Phys. Rev. B* **102**, 085412 (2020).

- [25] E. J. König, M. T. Randeria, and B. Jäck, Tunneling Spectroscopy of Quantum Spin Liquids, *Phys. Rev. Lett.* **125**, 267206 (2020).
- [26] J. Feldmeier, W. Natori, M. Knap, and J. Knolle, Local probes for charge-neutral edge states in two-dimensional quantum magnets, *Phys. Rev. B* **102**, 134423 (2020).
- [27] Y. Yamaji, T. Suzuki, T. Yamada, S.-I. Suga, N. Kawashima, and M. Imada, Clues and criteria for designing a Kitaev spin liquid revealed by thermal and spin excitations of the honeycomb iridate Na_2IrO_3 , *Phys. Rev. B* **93**, 174425 (2016).
- [28] S. K. Choi, R. Coldea, A. N. Kolmogorov, T. Lancaster, I. I. Mazin, S. J. Blundell, P. G. Radaelli, Y. Singh, P. Gegenwart, K. R. Choi, S.-W. Cheong, P. J. Baker, C. Stock, and J. Taylor, Spin Waves and Revised Crystal Structure of Honeycomb Iridate Na_2IrO_3 , *Phys. Rev. Lett.* **108**, 127204 (2012).
- [29] A. Banerjee, C. A. Bridges, J.-Q. Yan, A. A. Acze, L. Li, M. B. Stone, G. E. Granroth, M. D. Lumsden, Y. Yiu, J. Knolle, S. Bhattacharjee, D. L. Kovrizhin, D. A. T. R. Moessner, D. G. Mandrus, and S. E. Nagler, Proximate Kitaev quantum spin liquid behaviour in a honeycomb magnet, *Nat. Mater.* **15**, 733 (2016).
- [30] S.-Q. Jia, Y.-M. Quan, L.-J. Zou, and H.-Q. Lin, Topological quantum phase transitions of anisotropic antiferromagnetic Kitaev model driven by magnetic field, *Ann. Phys. (Berlin)* **534**, 2200012 (2022).
- [31] J. Knolle, D. L. Kovrizhin, J. T. Chalker, and R. Moessner, Dynamics of a Two-Dimensional Quantum Spin Liquid: Signatures of Emergent Majorana Fermions and Fluxes, *Phys. Rev. Lett.* **112**, 207203 (2014).
- [32] J. Knolle, *Dynamics of a Quantum Spin Liquid* (Springer-Verlag, Heidelberg, Berlin, 2016).
- [33] See Supplemental Material at <http://link.aps.org/supplemental/10.1103/PhysRevResearch.4.023251> for the formula derivation of tunneling current, Green's functions of two SC leads, and dynamical spin correlations of anisotropic Kitaev QSLs.